論文 95-2-2-17

환형띠 조각면을 이용한 원형 축전기 해석

正會員 具 本 熙*, 金 彩 英**

A Solution Procedure for Round Disk Capacitor by using Annular Patch Subdomains

Bon Hee Koo*, Che Young Kim** Regular Members

要 約

원형축전기의 전하분포 및 용량계산을 위한 수치해석법이 제안되었다. 축전기 표면상의 등가 면전하분포 산출을 위해 모멘트법이 적용되었다. 본 방법에서는 축전기의 표면을 환형띠로 모델링하여 삼각형이나 사각형으로 모델링할 때에 발생하는 discretizing 오차를 없앴을뿐만 아니라 결과해의 정확도와 행열차수의 감소로 인한 계산 시간을 크게 향상시킬수 있었다. 계산된 전전하 분포로부터 축전기의 자유 면전하 및 구속 면전하를 산출하였고 축전기의 등전위선을 구하였다. 결과해의 타당성을 보이기 위해 원형 디스크 및 유전체로 채워진 축전기에 본 방법을 적용하여 계산된 결과를 분석하였다.

ABSTRACT

A numerical method is presented for determining the static charge distribution and capacitance of a round disk capacitor. Based on equivalent surface charge distributions, an integral equation subject to the boundary conditions is transformed into an algebraic equation by using method of moment. In the employed numerical scheme, annular patch subdomains are introduced not only to completely eliminate the discretizing errors often encountered in other triangular or rectangular techniques but also to improve the accuracy of solutions and to reduce the matrix size of resultant equation. By solving the transformed algebraic equation the total charge density consisting of free and bound charge density is numerically calculated, thereby the equipotential lines around a round disk capacitor are obtained.

To show the usefulness of this method the employed scheme is applied to a single round disk with an exact solution and to the dielectric filled capacitor partially covered by plates. The numerical results are examined and discussions are also made to support the validity of the presented scheme.

*한국전자통신연구소 연구원
**경북대학교 전자공학과 교수
論文番號 : 94277
接受日字 : 1994年 10月 7日

I. Introduction

Evaluation of a capacitance for a round disk capacitor has been studied by many authors[1-4] who were willing to take into account the fringing field effects. For this most of all used the numerical method in which the surfaces are divided into triangular or rectangular patches depending on the geometry, and on these patches the charge densities assumed to be uniform[5,6]. However, either of these methods may yield too big matrix size or poor accuracy if they are applied to a round disk capacitor due to their discretizing scheme taken. To a good approximation, choosing a well matched patch shapes suitable to the given geometry makes a sense because the resultant matrix size or solution accuracy will be greatly dependent on the patch shapes taken.

In this paper, a capacitance and an equipotential line are numerically calculated. For the capacitance of a round disk capacitor filled with a finite dielectric slab the equivalent surface charges are put on the top and bottom plates as of free charges and on the dielectric boundary as of bound charges, thereby the integral equation to be solved can be represented by a free space Green's function. As prescribed boundary conditions two potentials on the top and bottom plates and the continuity of electric flux density across the dielectric layer were incorporated into the free space integral equation. To determine the equivalent surface charge densities lying on two plates and dielectric layer this integral equation is solved by the moment methods.

In an application of moment methods the plates are subdivided into annular patches, and the dielectric layer into rings on which the charge densities are assumed to be constant. Expansion functions for the charge densities are taken as annular pulses whereas testing functions are chosen as tubes with zero thickness width going around the center of the divided patches, which eventually reaches to a point matching technique. By introducing these annular patch subdomain the discretizing errors arson in divided round surfaces could be completely removed, which was often encountered in other shapes including a triangular or rectangular patch etc. Hence by employing this scheme not only the accuracy of numerical solutions but also the matrix size of a resultant algebraic equations are greatly reduced compared to those of the rectangular or triangular subsections.

Once determining the equivalent surface charge densities the capacitance and the equipotential lines could be numerically computed. By superposing the potential contributions by the annular patch subsections the equipotential lines are drawn around a capacitor. The accuracy of a numerical solutions is confirmed by comparing them to the known exact solution for a single disk capacitor and to the reported solution for a round disk capacitor.

II. Formulation of the Problem

Fig. 1 shows a round disk capacitor filled with a homogeneous dielectric medium of dielectric constant ϵ_r, and the top and bottom plate keep to maintain the potential difference V_1 and V_2 respectively. In here a denotes a radius of a round disk capacitor, W the dielectric slab width, and h the height between top and bottom conductors. The solution procedure is based on the method of replacing all the conducting surfaces and dielectric layers with equivalent layers of unknown charge densities in free spaces[7]. With this replacement, the potential and electric flux density of a round disk capacitor are given by

$$V(\underline{r}) = \frac{1}{4\pi\varepsilon_0} \int\int_S \frac{\sigma_T(\underline{r}')}{|\underline{r}-\underline{r}'|} dS' \tag{1}$$

$$\underline{D}(\underline{r}) = -\varepsilon \nabla V(\underline{r}) \tag{2}$$

where S is the surface of the round disk capacitor, and V the potential by the charges and $\underline{D}$ the electric flux density vector. And also $\sigma_T(\underline{k})$ represents the total charge density composed of free charge lying on the plates and bound charge on the dielectric to dielectric interface. ε and ε_0 are the permittivity of a material and a vacuum respectively.

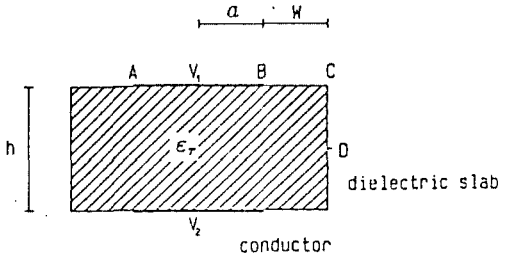

Fig. 1. Cross section of a round disk capacitor with dielectric slab.

Applying the potential boundary conditions to the top and bottom plates the potential in eqn.(1) reduces to V_i for i=1 and 2. To evaluate eqn.(2) along the medium interface this equation is decomposed into two parts, one with the self term and the other with the mutual contribution term.

$$\underline{D}^{\pm} \cdot \hat{n} = D_n^{\pm}(self) + D_n^{\pm}(PV) \tag{3-1}$$

where

$$D_n^{\pm}(self) = \begin{cases} \varepsilon^{+} \dfrac{\sigma_T}{2\varepsilon_0} & \text{for exterior region} \\ -\varepsilon^{-} \dfrac{\sigma_T}{2\varepsilon_0} & \text{for interior region} \end{cases} \tag{3-2}$$

$$D_n^{\pm}(PV) = \frac{\varepsilon^{\pm}}{4\pi\varepsilon_0} PV \int\int_S \frac{(\underline{r}-\underline{r}')\cdot\hat{n}}{|\underline{r}-\underline{r}'|^3} \sigma_T(\underline{r}') dS' \tag{3-3}$$

In here $PV\iint$ denotes the principal value of the integration. The superscripts(+) and (-) represent the exterior and interior region of the medium. $\hat{n}$ is an outward normal vector directed to the exterior region. When eqn.(3) is applied to a zero thickness conductor the free charge density σ_f and the total charge density σ_T are related by

$$\begin{aligned} \Delta D &= (\underline{D}^{+} - \underline{D}^{-}) \cdot \hat{n} \\ &= D_n^{+}(PV) - D_n^{-}(PV) + \frac{\varepsilon^{+}+\varepsilon^{-}}{2\varepsilon_0}\sigma_T \\ &= \sigma_f . \end{aligned} \tag{4}$$

For a dielectric to dielectric boundary with no conductor present ΔD becomes zero.

Once determining the total surface charge density the free charge density can be calculated by eqn.(4). By applying eqn.(4) to a dielectric to dielectric interface the bound charge density σ_b lying on that boundary is given by

$$\sigma_b = \frac{\varepsilon^{-}-\varepsilon^{+}}{\varepsilon^{+}} \underline{D}^{+} \cdot \hat{n}. \tag{5}$$

The total surface charge density σ_T is numerically obtained by the method of moments. A set of expansion functions $\{f_n(\underline{r}); n=1,2,\cdots,M\}$ is chosen and the charge density on surface is expanded in terms of the chosen expansion functions

$$\sigma_T = \sum \sigma_{Tn} f_n(\underline{r}) \tag{6}$$

where $f_n(\underline{r})$ has a unit height on the nth annular patch subdomains and zero otherwise. σ_{Tn}'s are the expansion coefficients of the charge densities to be determined. A number $M=N_c+N_d$ is the total number of subsections, in which N_c means the number of subdomains on the plates and N_d for the number on the dielectric to dielectric interface. The total M equation is needed to solve for σ_{Tn} for which N_c equations are obtained

by applying the potential boundary conditions on the plates, and the remaining N_d equations by applying the continuity of normal components of the electric flux density on the dielectric interface. Substituting eqn.(6) into (1) and (4) on which the potentials were set to V_i and the free charge density σ_f set to zero, and testing the resulting equation with each thin tube weighting functions we obtain

$$\begin{bmatrix} \Phi_m(f_n) \\ \cdots \\ \Delta D_m(f_n) \end{bmatrix} \begin{bmatrix} \sigma_{Tn} \end{bmatrix} = \begin{bmatrix} V_i \\ \cdots \\ 0 \end{bmatrix} \tag{7-1}$$

where

$$\Phi_m(f_n) = \frac{1}{4\pi\varepsilon_0} \int\int_{\Delta S_n} \frac{dS}{|\underline{r}_m - \underline{r}_n|} \tag{7-2}$$

for $m=1,2,\cdots,N_c$ and $n=1,2,\cdots,M$, and

$$\Delta D_m(f_n) = \frac{(\varepsilon^+ - \varepsilon^-)}{4\pi\varepsilon_0} \int_{\Delta S_n} \frac{(\underline{r}_m - \underline{r}_n)\cdot \hat{n}_m}{|\underline{r}_m - \underline{r}_n|^3} dS \tag{7-3}$$

for $m=N_c+1,\cdots,M$ and $n=1,2,\cdots,M$. ΔS_n denotes the annular subsection, and the homogeneous dielectric medium was assumed in the derivation. The matrix elements $\Phi_m(f_n)$ in eqn.(7-2) may be regarded as a potential at the testing point due to a uniform surface charge density ΔW_n over the nth annular ring with radius ρ_n.

Once determining the total surface charge density by the matrix inversion on eqn.(7) the free charge densities on either plates can be specified by using eqn.(4). Hence from the total free charge Q and the potential difference V between the plates the capacitance of a round capacitor can be found to be

$$C = \frac{Q}{V} = \left| \frac{1}{V_2 - V_1} \sum_{n=1}^{N_c^t} \sigma_{fn} \Delta S_n \right| = \left| \frac{1}{V_2 - V_1} \sum_{n=N_c+1}^{N_c} \sigma_{fn} \Delta S_n \right| \tag{8}$$

where the superscript t in N_c^t means top plate. In eqn.(8) the numerator of third term represents the total free charge on top plate whereas the fourth term indicates the total free charge on bottom plate.

Ⅲ. Evaluation of Matrix Elements

Fig. 2 shows the coordinates for evaluating matrix elements in eqn.(7). By taking into account a symmetry of the geometry a testing point is chosen to lie on the xz plane for computational convenience. In those case we recognize that the distant vector $\underline{r}_m$ and $\underline{r}_n$ are

$$\begin{aligned} \underline{r}_m &= \hat{x}_0 \rho_m + \hat{z}_0 h_m \\ \underline{r}_n &= \hat{x}_0 \rho_n \cos\phi' + \hat{y}_0 \rho_n \sin\phi' + \hat{z}_0 h_n \end{aligned} \tag{9-1}$$

where ϕ' is an angle between the x axis and radial distance ρ_n. The distance $|\underline{r}_m - \underline{r}_n|$ from a testing point $\underline{r}_m$ to source point $\underline{r}_n$ is

$$|\underline{r}_m - \underline{r}_n| = \sqrt{\rho_m^2 + \rho_n^2 + (h_m - h_n)^2 - 2\rho_m \rho_n \cos\phi'}. \tag{9-2}$$

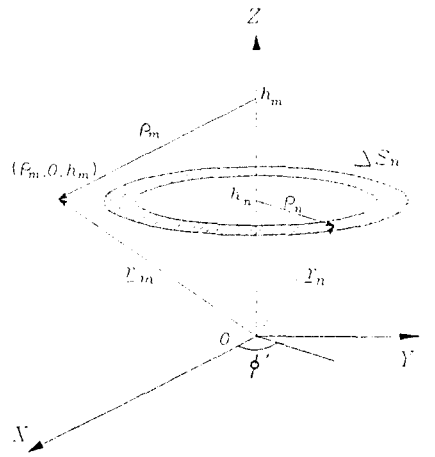

Fig. 2. The coordinates for evaluating the matrix elements.

We evaluate the integral in eqn.(7-2) by substituting (9-2)

$$\Phi_m(f_n) = \frac{\rho_n \Delta W_n}{2\pi\varepsilon_0} \int_0^{\pi} \frac{d\phi'}{\sqrt{\rho_m^2+\rho_n^2+(h_m-h_n)^2-2\rho_m\rho_n\cos\phi'}} = \frac{\rho_n \Delta W_n}{\pi\varepsilon_0 A_{mn}} K(k_{mn}) \tag{10-1}$$

where

$$K(x) = \int_0^{\pi/2} \frac{d\phi}{\sqrt{1-x^2\sin^2\phi}} \tag{10-2}$$

$$A_{mn}^2 = (\rho_m+\rho_n)^2+(h_m-h_n)^2 \tag{10-3}$$

$$k_{mn}^2 = \frac{4\rho_m\rho_n}{A_{mn}^2} < 1 . \tag{10-4}$$

ΔW_n represents the width of each annular patch with a surface ΔS_n as shown in Fig. 2. In the derivation of eqn.(10) a new integral variable $\phi = (\pi - \phi')/2$ was introduced. $K(x)$ in eqn.(10-2) is a complete elliptic integral of the first kind.

For nonoverlapped pulse portions $(m \neq n)$ the argument x in $K(x)$ lies between 0 and 1 as described in eqn.(10-4), hence eqn.(10) can be computed by a numerical integral technique without a difficulty. For the coincident pulse portion $(m=n)$ the integral is evaluated analytically. For this the nth annular section is divided into two parts, on including a singular point and the other not. The integral contributed by a singular point will be performed over an approximate square area ΔW_n^2. In other words by taking the angle $\theta = \Delta W_n/\rho_n$ which yields an approximate square area around a singular point, the integral along the annular ring is separated into one ranging from $-\theta/2$ to $\theta/2$ and the other from $\theta/2$ to $2\pi-\theta/2$. After setting $\rho_m=\rho_n$ in eqn.(9-2) and substituting this result into eqn.(7-2) shows

$$\Phi_m(f_n) = \frac{1}{4\pi\varepsilon_0} \int_{-\Delta W_n/2}^{\Delta W_n/2} \int_{-\Delta W_n/2}^{\Delta W_n/2} \frac{dxdy}{\sqrt{x^2+y^2}} + \frac{\Delta W_n}{4\pi\varepsilon_0} \int_{\theta/2}^{2\pi-\theta/2} \frac{d\phi'}{\sqrt{2}\sqrt{1-\cos\phi'}} = \frac{\Delta W_n}{\pi\varepsilon_0} \ln(1+\sqrt{2}) + \frac{\Delta W_n}{2\pi\varepsilon_0} \ln(\cot(\theta/8)). \tag{11}$$

In here the first term is a contribution by a singular point and the second term by the remaining parts, and ln denotes the natural logarithm.

$\Delta D_m(f_n)$ in eqn.(7-3) has to be evaluated over the plates and over the dielectric interfaces. We'll denote the former by $\Delta D_m(f_n)_z$ and the latter by $\Delta D_m(f_n)_x$ since the unit testing point vector $\hat{n}m$ directs toward $\pm\hat{z}_0$ direction over the plates and $\hat{x}_0$ direction over the dielectric interfaces when the testing point lies in the xz plane. ε^+ and ε^- will be replaced by ε_0 and $\varepsilon_0\varepsilon_r$ respectively, and the relation $\phi = (\pi-\phi')/2$ will be used for computational purpose. To evaluate $\Delta D_m(f_n)_x$ for the mutual term $(m \neq n)$ incorporating $(\underline{r}_m - \underline{r}_n) \cdot \hat{z}_0 = h_m - h_n$ and eqn.(9-2) into (7-3) shows

$$\Delta D_m(f_n)_z = \frac{(1-\varepsilon_r)\rho_n(h_m-h_n)\Delta W_n}{\pi A_{mn}^3} \int_0^{\pi/2} \frac{d\phi}{(1-k_{mn}^2\sin^2\phi)^{3/2}} = \frac{(1-\varepsilon_r)\rho_n(h_m-h_n)\Delta W_n}{\pi A_{mn}^3} \frac{E(k_{mn})}{1-k_{mn}^2} \tag{12-1}$$

where

$$E(x) = \int_0^{\pi/2} \sqrt{1-x^2\sin^2\phi}\, d\phi. \tag{12-2}$$

$E(x)$ is a complete elliptic integral of the second kind. For the self term $(m=n)$, the subsection is divided into two parts including a singular point and the remaining parts, as done for obtaining eqn.(11), and the integral is carried out for each part. Then $\Delta D_m(f_n)_z$ simply becomes

$$\Delta D_m(f_n)_z = \frac{1+\varepsilon_r}{2} \tag{12-3}$$

since the vector $(\underline{r}_m - \underline{r}_n)$ and $\hat{n}_m$ are orthogonal to each other in eqn.(7-3). Therefore the contribution is only the part including the singular point for this case.

To calculate $\Delta D_m(f_n)_x$ for the mutual term substituting the relation $(\underline{r}_m-\underline{r}_n)\cdot\hat{x}_0=\rho_m-\rho_{mn}\cos\phi'$ and eqn.(9-2) into (7-3) yields

$$\Delta D_m(f_n)_x = \frac{1-\varepsilon_r}{4\pi}\int_{-\Delta W_n/2}^{\Delta W_n/2}\rho_n d\rho \int_0^{2\pi}\frac{\rho_m-\rho_n\cos\phi'}{[\rho_m^2+\rho_n^2+(h_m-h_n)^2-2\rho_m\rho_n\cos\phi']^{3/2}}d\phi'$$
$$= \frac{(1-\varepsilon_r)\rho_n(\rho_m+\rho_n)\Delta W_n}{\pi A_{mn}^3}\int_0^{\pi/2}\frac{d\phi}{(1-k_{mn}^2\sin^2\phi)^{3/2}} \quad (13\text{-}1)$$
$$-\frac{2(1-\varepsilon_r)\rho_n^2\Delta W_n}{\pi A_{mn}^3}\int_0^{\pi/2}\frac{\sin^2\phi}{(1-k_{mn}^2\sin^2\phi)^{3/2}}d\phi$$
$$= \frac{(1-\varepsilon_r)\rho_n^2\Delta W_n}{\pi A_{mn}^3}\left[\left(1+\frac{\rho_m}{\rho_n}-\frac{2}{k_{mn}^2}\right)\frac{E(k_{mn})}{1-k_{mn}^2}+\frac{2}{k_{mn}^2}K(k_{mn})\right]$$

$K(x)$ and $E(x)$ were defined in eqn.(10-2) and (12-2) respectively. For the self term, similar procedure is carried out to evaluate $\Delta D_m(f_n)$, as done for obtaining eqn.(12-3). For this case the contribution of the remaining parts is evaluated analytically, since the $(\underline{r}_m-\underline{r}_n)$ and $\hat{x}_0$ over this section is not orthogonal to each other. Hence the expression on $\Delta D_m(f_n)_x$ for a self term becomes

$$\Delta D_m(f_n)_x = \frac{(1-\varepsilon_r)\rho_m\Delta W_n}{4\pi}\int_{\theta/2}^{2\pi-\theta/2}\frac{\rho_m(1-\cos\phi')}{(\sqrt{2}\rho_m\sqrt{1-\cos\phi'})^3}d\phi'+\frac{1+\varepsilon_r}{2}$$
$$= \frac{(1-\varepsilon_r)\Delta W_n}{4\pi\rho_m}\ln(\cot(\theta/8))+\frac{1+\varepsilon_r}{2} \quad (13\text{-}2)$$

By putting the matrix elements given by eqn.(10), (11), (12), and (13) into eqn.(7) the charge density σ_{Tn} can be determined.

Once determining the total charge distributions by using eqn.(7) the electric potential $V(\underline{r})$ at the field point $\underline{r}$ can be computed by superposing the potential contributions in terms of segment charges lying on the annular patches, which is written as

$$V(\underline{r})=\sum_{n=1}^{M}\phi^a(\underline{r}:\underline{r}_n) \quad (14)$$

where, $\phi^a(\underline{r}:\underline{r}_n)$ is a potential due to the nth annular subsection with charge density σ_{Tn}. From eqn.(14) the equipotential lines can be drawn around the capacitor.

Ⅳ. Numerical Examples

To show the validity and usefulness of our numerical scheme we applied this method to a single round disk with radius a which was charged to a constant potential V_0. The accurate charge density distribution on this disk is given by[8]

$$\sigma(\rho)=\frac{4V_o\varepsilon_o}{\pi\sqrt{a^2-\rho^2}} \quad (15)$$

where ρ is the distance from the center of the disk. The capacitance of the disk is $8\varepsilon_0 a$. For a numerical solution, the disk is divided into M equidistant annular patch subsections and on each subsections the constant charge density distribution was assumed. Fig. 3 shows an excellent agreement between the exact and computed charge density distribution for M=30. This graph shows a singular behavior at the disk edge as expected in eqn.(15). The computed solution is getting convergent to the exact solution by increasing the number of annular subsections. In Table I numerically calculated capacitance of a single round disk with respect to the number of employed subsections are presented for comparison between the annular and triangular subsections[9]. The data in Table I is the normalized capacitance C/a. The relative errors are less than 1% for a matrix size 20 and 0.5% for 40 respectively. As shown in this table results by annular patch subsections show much smaller errors than those of triangular patches for the same matrix size.

The round disk capacitor we wish to consider was shown in Fig. 1. Fig. 4 shows the

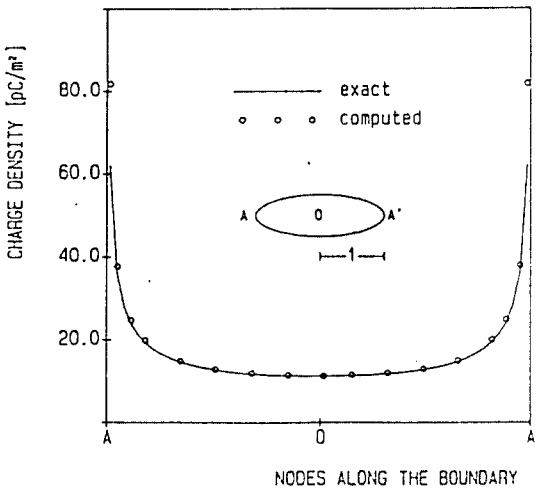

Fig. 3. Exact and computed charge density distributions of a single round disk (a=1, V_0=1V).

Table I. Normalized capacitance of a single round disk(pF/m).

Annular patch			Triangular patch[9]		
M	C/a	%error	M	C/a	%error
10	69.57	1.76	18	59.80	15.57
15	70.01	1.16	30	61.10	13.74
20	70.22	0.86	42	61.80	12.75
25	70.35	0.68	54	62.24	12.13
30	70.43	0.56	60	66.03	6.78
40	70.55	0.41	84	66.72	5.72
exact	70.83				

charge distribution of a round disk capacitor for W=0 in Fig. 1. In this figure we set the radius a and height h to be unity, and voltages to be V_1=-V_2=1[V]. The value by dotted white (∘ ∘ ∘) represents the total charge density distribution for ε_r=1 and the other graphs show the distribution for ε_r=3.0. The ratio between the total charge to free charge was about 2.2 for ε_r=3.0. For small h/a ratio, the ratio of total to free charge is nearly unity and eventually the fringing field has little significance. Along the boundary AB, the positive free charge density and negative bound charge density due to the induced polarization charges were appeared as expected since the potential of a upper plate is higher than a lower plate. The discontinuity of a bound charge at the corner of a capacitor, marked B in Fig.4, is due to the free positive charge on the top plate and positive bound charge lying on the boundary BC. The bound charges lying along BCD are responsible for the fringing field effects. So they cause to bend the equipotential lines across the dielectric interfaces.

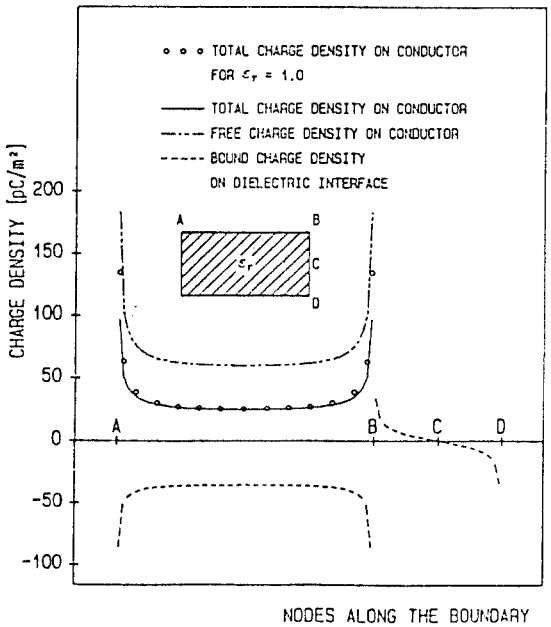

Fig. 4. Charge density distribution of a round disk capacitor.

Fig. 5 shows the equipotential lines on the xz plane. The lines are nearly parallel to each other in the interior region, but somewhat bent at the corner due to the fringing field effect. At the corner the lines for ε_r=3.0 are more parallel than those for ε_r=1.0. This happens since the fringing field becomes smaller for bigger ε_r. However, the equipotential lines for ε_r=3.0 show sharp bending at the boundary(x=1) because the electric flux is discontinuous at a

dielectric to dielectric interface due to the bound charges in there.

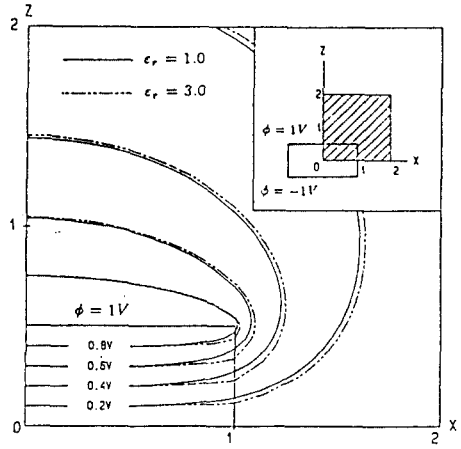

Fig. 5. Equipotential lines of a round disk capacitor.

Fig. 6 represents the capacitance of a round disk capacitor as a function of h/a for ϵ_r=1.0 and 3.0 respectively, and together with results by Shen's formula[4]

$$C = \varepsilon_r \frac{\varepsilon_o \pi a^2}{h}\left[\ 1+\frac{2h}{\pi\varepsilon_r a}\left\{\ln\left(\frac{\pi a}{2h}\right)+1.7726\right\}\right] \quad (16)$$

Shen's formula is well suited only for h/a<1 since it was obtained under the first order approximation.

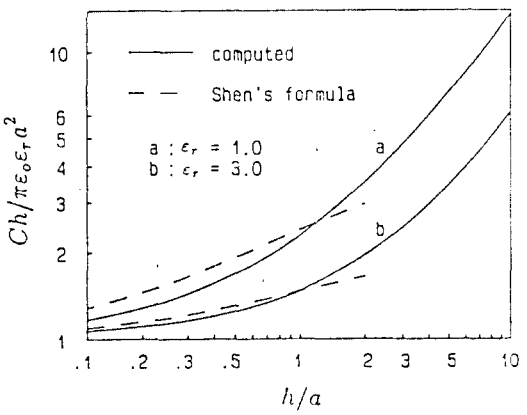

Fig. 6. Normalized capacitance vs parameter h/a.

Fig.7 represents the normalized capacitance for a round disk capacitor by changing parameter W for ϵ_r=3.0. W is the dielectricslab width shown in Fig.1. In this figure as the uncovered dielectric slab width W is increasing the corresponding capacitance is slightly increased, thereby the fringing field effect becomes somewhat more evident.

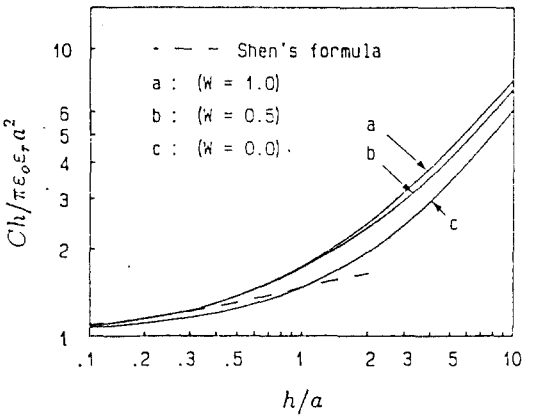

Fig. 7. Normalized capacitance vs parameter h/a by changing parameter $W(\epsilon_r$=3.0).

V. Conclusion

A solution procedure to analyze a round disk capacitor was introduced by using annular patch subdomains. Based on this technique the discretizing errors on the capacitor surfaces could be completely removed, which lead us to have more accurate numerical results together with saving on computation time and memory as well. For numerical calculation pulses on the annular patches were taken as the expansion functions and zero thickness thin tubes were chosen as the testing functions, which eventually led to a point matching.

To show the effectiveness on the proposed scheme this technique was applied to a single round disk and a capacitor filled with a dielectric slab covered by the partial plates. The calculated capacitance's for these structures

showed good agreement with known solutions. By drawing the equipotential lines around the capacitor discussions were also made on the resultant fringing field effects related to the bound charge densities lying on the dielectric interfaces.

References

1. A. Farrar and A. T. Adams, "Matrix methods for microstrip three-dimensional problems," *IEEE Trans. Microwave Theory Tech.*, vol. MTT-20, pp. 497-504, Aug. 1972.
2. P. Benedex and P. Silvester, "Capacitance of parallel rectangular plates separated by a dielectric sheet," *IEEE Trans. Microwave Theory Tech.*, vol. MTT-20, pp. 504-510, Aug. 1972.
3. T. Itoh and R. Mittra, "A new method for calculating the capacitance of a circular disk for microwave integrated circuit," *IEEE Trans. Microwave Theory Tech.*, vol. MTT-21, pp. 431-432, June 1973.
4. L. C. Shen, S. A. Long, M. R. Allerding, and M. D. Walton, "Resonator frequency of a circular disc, printed circuit antenna," *IEEE Trans. Antennas Propagat.*, vol. AP-25, pp. 595-596, July 1977.
5. R. F. Harrington, *Field Computation by Moment Method*, N.Y. Macmillan Co., pp. 24-28, 1968.
6. D. K. Reitan, "Accurate determination of the capacitance of rectangular parallel-plate capacitor," *Journ. Appl. Phys.*, vol.30, no.2, pp. 172-176, Feb. 1959.
7. J. A. Stratton, *Electromagnetic Theory*, New York : McGraw-Hill, pp. 183-185, 1941.
8. W. R. Smythe, *Static and Dynamic Electricity*, New York : McGraw-Hill, p. 114, 1950.
9. S. M. Rao, A. W. Glisson, D. R. Wilton and B. S. Vidula, "A simple numerical solution procedure for static problems involving arbitrary-shaped surface," *IEEE Trans., Antennas Propagat.*, vol. AP-27, No. 5, pp. 604-608, Sept. 1979.

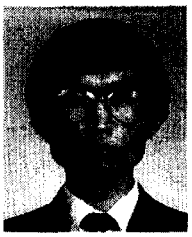

具本熙 Bon Hee Koo)
1966년 5월 1일생
1988년 : 경북대학교 전자공학과 졸업 (공학사)
1990년 : 경북대학교 대학원 전자공학과 졸업(공학석사)
1990년~현재 : 한국전자통신연구소 정보통신표준연구센터 연구원
※ 주관심분야 : 무선 인터페이스 표준 연구분야, 마이크로파 공학 및 전자파 수치해석등임.

金彰英 (Che Young Kim)
1953년 3월 10일생
1976년 2월 : 경북대학교 전자공학과 졸업
1978년 2월 : 한국과학원 전기 및 전자공학과(공학석사)
1990년 2월 : 한국과학기술원 전기 및 전자공학과(공학박사)
1979년~현재 : 경북대학교 전자공학과 교수
1985년 9월~1986년 8월 : 미국 Syracuse 대학 연구교수
1991년 9월~1993년 2월 : 미국 MIT 공대 연구과학자
※ 주관심분야 : 차량 및 건물에 부착된 안테나 특성 및 건물 내부의 전계계 계산.
매몰된 물체의 탐지 및 컴퓨터 코드 개발, 복잡한 구조물의 산란파 해석 및 특징변수 추출, 이동통신, 전자파 이론 및 응용 등임.